Accelerated Publications

The Function of Photosystem I. Quantum Chemical Insight into the Role of Tryptophan−Quinone Interactions†

Martin Kaupp*

Institut für Anorganische Chemie, Universität Würzburg, Am Hubland, D-97074 Würzburg, Germany

Received November 26, 2001; Revised Manuscript Received January 22, 2002

ABSTRACT: Quantum chemical calculations have provided evidence for the role of tryptophan residues in the electron transfer process of photosystem I (PS-I). The interaction of Trp with quinone acceptors and their radical anions in the A_1 site of PS-I has been modeled by various indole−quinone and indole−semiquinone complexes. MP2 optimizations show that, while neutral quinones and an indole molecule prefer a π-stacked arrangement, semiquinone radical anions prefer a T-stacked conformation with significant N−H···π hydrogen bonding interactions. Comparison of density functional calculations of electronic **g**-tensors with electron paramagnetic resonance data strongly suggests that hydrogen-bonded T-shaped arrangements occur upon reduction of quinone acceptors without an extended side chain (e.g., duroquinone or naphthoquinone), when reconstituted into the phylloquinone-depleted A_1 site of PS-I. In contrast, for the native phylloquinone (vitamin K_1, Q_K), reorientation of the semiquinone radical anion is prevented by side chain−protein interactions. For a fixed π-stacked arrangement, the extent of the intermolecular interaction is reduced upon one-electron reduction. This corresponds to a lowering of the redox potential of the $P_{700}^{+\bullet}Q_K^{-\bullet}$ radical pair, due to interactions of Q_K with a tryptophan. Together with the comparably weak hydrogen bonding in PS-I, the proposed model explains the very negative redox potential of the A_1 site, needed for forward electron transfer. T-stacking hydrogen bonds to semiquinones may also have to be considered in many other electron transfer processes in living organisms.

Photosynthetic reaction centers convert sunlight into chemical energy. The initial steps of the photosynthetic electron transfer chain involve generally the transfer of an electron from an electronically excited chlorophyll molecule to a quinone. In different reaction centers, nature is able to widely vary the redox potential of the quinone acceptor and thus the rate and direction of further electron transfer. This is done by adjusting the interactions of quinones and of their semiquinone radical anions with the protein environment. In particular, the quinone binding site (A_1 site) in photosystem I (PS-I)[1] of plants and cyanobacteria produces a very negative redox potential (*1*, *2*).

Transient EPR of the $P_{700}^{+\bullet}Q^{-\bullet}$ charge-separated biradical state revealed very unusual spectra, when duroquinone (DQ) or naphthoquinone (NQ), i.e., quinones without extended side chain, were reconstituted into the phylloquinone-depleted A_1 site of PS-I (*3*). The EPR data indicate that the foreign semiquinones are bound to the A_1 site, but their orientation differs from that of the radical anion of the native phylloquinone (vitamin K_1, abbreviated as Q_K) (*3*, *4*). Compared to the **g**-shift tensors, $\Delta\mathbf{g}$, of $DQ^{-\bullet}$ or $NQ^{-\bullet}$ in an isotropic 2-propanol solution (*5*) or in the active sites of reaction centers of purple bacteria (*4*), the Δg_x components in these preparations are increased by ∼25−30%, and the Δg_y components even by ∼33−43% (Table 1). In contrast, in high-field EPR spectra of photoaccumulated $Q_K^{-\bullet}$ (*6*), or in transient EPR spectra (*7*) of $P_{700}^{+\bullet}Q_K^{-\bullet}$ in unmodified PS-I, the Δg_x and Δg_y components are enhanced only by ∼17 and ∼4%, respectively, compared to those in an isotropic 2-propanol solution (Table 1).

How can these dramatic differences between native PS-I and the reconstituted preparations be explained? Recent systematic quantum chemical calculations of **g**-tensors for an extended series of semiquinone radical anions (*8*), using a new density functional theory (DFT) approach (*9*), showed that the experimental Δg_x and Δg_y components measured in frozen 2-propanol could be reproduced essentially to within experimental accuracy. Quantum chemical calculations thus now offer the possibility of evaluating and predicting the **g**-shift tensors of semiquinone radical anions quantitatively also in protein environments. Hydrogen bonding is known

† This work was supported by Deutsche Forschungsgemeinschaft (priority program SPP1051 "High-Field EPR in Biology, Chemistry, and Physics") and by Fonds der chemischen Industrie.

* To whom correspondence should be addressed. Telephone: +49-931-888-5281. Fax: +49-931-888-7135. E-mail: kaupp@mail.uni-wuerzburg.de.

[1] Abbreviations: BQ, benzoquinone; CP, counterpoise (correction); DFT, density functional theory; DMF, dimethylformamide; DMNQ, dimethylnaphthoquinone; DQ, duroquinone (2,3,5,6-tetramethylbenzoquinone); EPR, electron paramagnetic resonance; ESEEM, electron spin−echo envelope modulation; Gly, glycine; Leu, leucine; MP2, second-order Møller−Plesset perturbation theory; nmf, *N*-methylformamide; NQ, naphthoquinone; PS, photosystem; P_{700}, primary chlorophyll donor of photosystem I; Q_K, vitamin K_1 (phylloquinone); Trp, tryptophan.

10.1021/bi0159783 CCC: $22.00
Published on Web 02/08/2002

Table 1: Experimental **g**-Shift Tensors (parts per million) for Semiquinone Radical Anions in Different Environments

semiquinone	environment	Δg_x	Δg_y	Δg_z
$DQ^{-\bullet}$	frozen 2-propanol (5)	3800	2800	−100
	PS-I (4)	5000	4000	0
$NQ^{-\bullet}$	frozen 2-propanol (5)	3500	2700	−40
	PS-I (4)	4400	3700	0
$Q_K^{-\bullet}$	frozen 2-propanol (5)	3320	2620	−150
	PS-I (6)	3900	2750	−140

to reduce both Δg_x and Δg_y. However, the calculations showed that even in the complete absence of hydrogen bonding, the Δg_y components of $DQ^{-\bullet}$, or even of unsubstituted benzosemiquinone ($BQ^{-\bullet}$), should never be much larger than 3000 ppm (*8*). This contrasts sharply with the large values measured (*3*, *4*) for $NQ^{-\bullet}$ or $DQ^{-\bullet}$ in the A_1 binding site of PS-I (Table 1), and it suggests that other interactions must influence the **g**-tensors of these particular systems. A nearby tryptophan (Trp) residue appeared to provide the most likely candidate for such extra interactions. The recent X-ray crystallographic analysis of the PS-I complex of *Synechococcus elongatus* at 2.5 Å resolution (*10*) has clearly confirmed the presence of a Trp residue (Trp A697[2]), which is π-stacked with the quinone acceptor (Q_K-A[2]). Previous evidence for the presence of Trp residues near the quinone acceptor sites has come from quinone reconstitution studies (*11*), from ESEEM spectroscopy (*12*), from modeling based on EPR data (*13*), and from site-directed mutagenesis work (*14*, *15*).

Here we employ large-scale post-Hartree−Fock ab initio MP2 quantum chemical calculations on quinone−indole and semiquinone−indole complexes to model the structures and energetics of Trp−Q and Trp−$Q^{-\bullet}$ interactions. This method includes electron correlation effects explicitly. It is expected to be at present the minimum quantum chemical level that covers the dispersion contributions to π-stacking interactions adequately, and the maximum level that is still applicable to realistic models of Trp−Q interactions. Subsequent DFT calculations of electronic **g**-tensors at the fully or partially optimized structures allow the direct check of various structural models against high-field EPR data. On the basis of the computed structures, binding energies, and electronic **g**-tensors, we propose a detailed model of how tryptophan residues are involved in the electron transfer process of PS-I.

COMPUTATIONAL METHODS

Structure and Energy Calculations. All structure optimizations and energy calculations employed the MP2 post-Hartree−Fock method, using the Gaussian 98 program (*16*), effective core potentials and DZP valence basis sets (*17*) for C, O, and N, and a DZV basis set for hydrogen (*18*). These medium-size basis sets were dictated by the large size of the more realistic model systems and by the available computational resources. Binding energies were corrected for basis set superposition errors (BSSE) by the full counterpoise (CP) method (*19*). The reliability of the results has been cross-checked by selected CP-corrected single-point MP2 calculations with larger 6-311+G** all-electron basis sets on BQ−indole and $BQ^{-\bullet}$−indole complexes (see below).

***g**-Tensor Calculations*. We employed MP2-optimized structures, or experimental intermolecular arrangements (*10*) combined with MP2-optimized substructures. All other details of the **g**-tensor calculations are as described in ref *8* (the underlying theory has been provided in more detail in ref *9*). Briefly, the calculations were carried out at the uncoupled DFT level with the BP86 functional (*20*, *21*) and DZVP basis sets (*18*), using the deMon program (*22*) and its **g**-tensor module (*9*). The spin−orbit operators were treated by the accurate all-electron atomic meanfield approximation (AMFI) (*23*, *24*; cf. ref *9*). A common gauge at the center of mass was employed (other choices, e.g., the center of the semiquinone ring, gave virtually identical results). For easier discussion of changes due to intermolecular interactions, we report **g**-shift tensors $\Delta\mathbf{g}$, defined as $\Delta\mathbf{g} = \mathbf{g} - g_e\mathbf{1}$ ($g_e = 2.002\,3219$), in parts per million (i.e., in units of 10^{-6}).

While DFT methods are presently not able to treat dispersion interactions adequately, previous studies have shown that they nevertheless provide good magnetic resonance parameters even of typical van der Waals complexes, when used with structures optimized at sufficiently high theoretical levels (*25*).

RESULTS AND DISCUSSION

Figure 1a shows the optimized structure for the 1:1 complex of benzoquinone (BQ) with indole. Even when a T-stacked, N−H···π-bonded structure was used as a starting point for the optimizations, the calculations converged to the π-stacked structure, in agreement with the observed arrangement in PS-I (*10*). The average optimized inter-ring distance is 3.01 Å, i.e., within the 3.0−3.5 Å range estimated from X-ray data for the Trp−Q_K distance in PS-I (*10*). The quinone ring eclipses the pyrrole ring of indole, with the N−H vector pointing roughly parallel to the bisector of the C1−C2 bond. The counterpoise (CP)-corrected MP2 binding energy for the complex is ∼14 kJ/mol (Table 2). When a perpendicular arrangement with an N−H···π bonding interaction was enforced in the optimizations (Figure 1b), the energy was ∼11 kJ/mol higher. Full optimizations for the DQ−indole and DMNQ−indole complexes also converged to the π-stacked arrangement (data not shown), with very similar interplane separations of 3.07 Å. The interaction energies in both of the larger complexes are calculated to be more than twice that for the BQ−indole complex (Table 2). This result suggests that the presence of methyl substituents and/or of a fused benzene ring connected to the quinone enhances van der Waals interactions significantly. The data show clearly that one function of the Trp residue is to bind to the quinone (*11*). They probably also explain why BQ has not been observed to bind to the A_1 site. MP2/6-311+G** single-point calculations on the optimized BQ−indole complex provide a higher binding energy (Table 2). This suggests that the standard level employed in this work underestimates the dispersion interactions at the π-stacked structures, due to the restricted basis sets.

In contrast to the neutral systems, the anionic semiquinone−indole complexes generally show a significant

[2] For the sake of brevity, we concentrate here exclusively on the amino acid residues of one of the two potential electron transfer branches (branch A). The X-ray structural data are very similar for the other branch (branch B) (*10*). Our choice does not imply a preference for a particular direction.

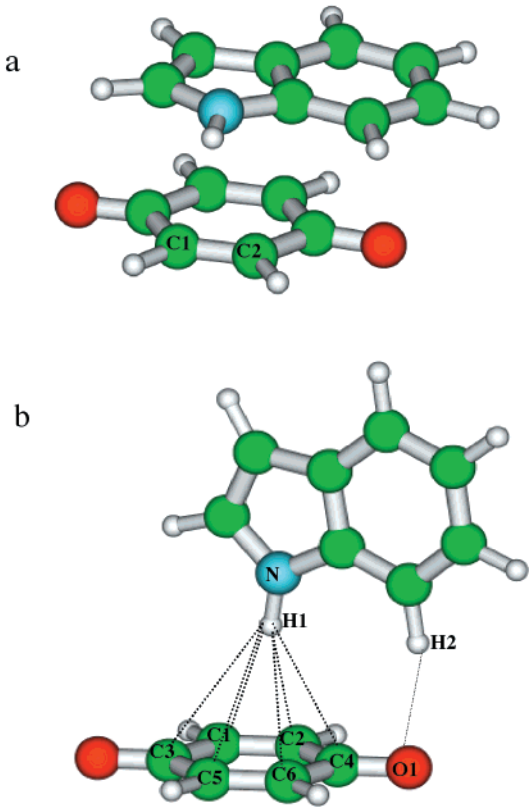

FIGURE 1: MP2-optimized structures of the BQ−indole neutral complex. (a) Fully optimized π-stacked structure (interplane distance of ~3.01 Å). (b) Constrained optimization result, with the indole plane forced to be perpendicular to the quinone plane. H-bond distances (in angstroms): H1···C1, 2.718; H1···C2, 2.604; H1···C3, 3.023; H1···C4, 2.799; H1···C5, 3.179; H1···C6, 3.082; and H2···O1, 2.583.

Table 2: Calculated Interaction Energies (kilojoules per mole)[a]

	Q−indole → Q + indole	$Q^{-\bullet}$−indole → $Q^{-\bullet}$ + indole
Q = BQ		
optimization	π-stacked, 14.7 (32.8[b]) T-stacked,[c] 3.5 (0.7[b])	T-stacked, 52.1 (57.4[b])
X-ray structure[d]	π-stacked, 13.0 (25.8[b])	π-stacked, 1.4 (15.4[b])
Q = DQ		
optimization	π-stacked, 32.0	T-stacked, 45.8
X-ray structure[d]	π-stacked, 23.8	π-stacked, 7.7
Q = DMNQ		
optimization	π-stacked, 32.1	T-stacked, 54.0
X-ray structure[d]	π-stacked, 30.1	π-stacked, 25.2

[a] Counterpoise-corrected MP2 results. [b] In parentheses is the 6-311+G** all-electron basis set result. [c] Restricted optimization with the indole ring forced to be perpendicular to the semiquinone ring. [d] Intermolecular distance and orientation as found in the X-ray structure analysis of PS-I (*10*), but fragment structures optimized at the MP2 level.

preference for a T-stacked N−H···π-bonded arrangement (shown in Figure 2 for the $DQ^{-\bullet}$−indole complex), with N−H···C contacts between 2.3 and 2.6 Å in length. Even optimizations starting from a perfectly parallel, π-stacked structure converged to this T-shaped arrangement. The intermolecular binding energies are similar for all three quinones, and they are remarkably large (Table 2). The CP-corrected MP2/6-311+G** single-point binding energy for the $BQ^{-\bullet}$−indole complex is only ~5 kJ/mol larger than that obtained at the standard computational level (Table 2),

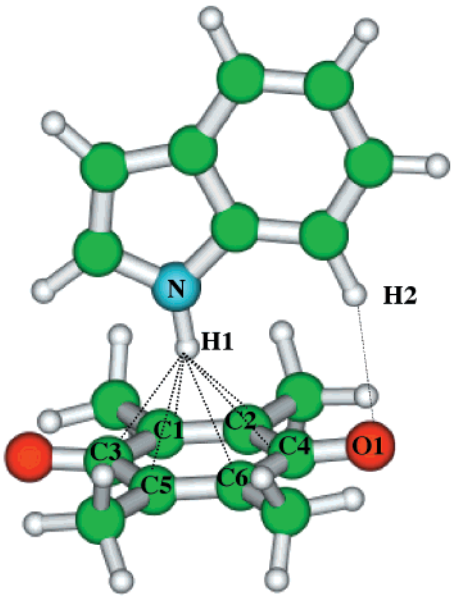

FIGURE 2: Fully MP2-optimized structure of the anionic $DQ^{-\bullet}$−indole complex. H-bond distances (in angstroms): H1···C1, 2.514; H1···C2, 2.551; H1···C3, 2.387; H1···C4, 2.494; H1···C5, 2.338; H1···C6, 2.376; and H2···O1, 2.593.

suggesting that basis set convergence of the binding energies is relatively fast for the T-stacked anionic complexes.

Single-point energy calculations with the standard basis have been carried out for indole−quinone and indole−semiquinone complexes at the experimentally determined π-stacked structure of the Trp−Q_K pair in PS-I (*10*) but with MP2-optimized intramolecular structure parameters for the neutral and anionic fragments, respectively (these parameters are expected to be significantly more accurate than the X-ray data). The resulting CP-corrected MP2 binding energies for the neutral complexes increase from ~13 kJ/mol for the BQ−indole complex to ~30 kJ/mol for the DMNQ−indole complex (Table 2). That is, they are only slightly smaller than the energies computed for the fully optimized systems. This suggests that the structural arrangement in PS-I is already optimized to provide strong π−π interactions for neutral quinones. In contrast, the anionic $BQ^{-\bullet}$−indole and $DQ^{-\bullet}$−indole complexes are bonded only weakly in this intermolecular orientation (Table 2). Binding in these $Q^{-\bullet}$−indole complexes is thus less favorable than for the neutral quinone. The computed binding energy for the $DMNQ^{-\bullet}$−indole complex corresponds only to a destabilization of ~5 kJ/mol relative to the neutral complex (Table 2). The large basis results for the BQ system indicate that basis set restrictions leave some uncertainty in the computed binding energies. With increasing computing power, a further refinement of these values will be possible in the future. We will also need to take into account hydrogen bonding, further electrostatic contributions, and vibrational effects for a more precise estimate. In any case, by forcing the $Q_K^{-\bullet}$ anion to stay essentially parallel to the nearby Trp, PS-I apparently is able to destabilize the semiquinone relative to the quinone state, and thus to lower the reduction potential of the $P_{700}^{+\bullet}Q_K^{-\bullet}$ radical pair.

In contrast, the computed interaction energies for the T-stacked radical anion $Q^{-\bullet}$−indole complexes are significantly larger than for the π-stacked neutral system (Table

Table 3: Calculated **g**-Shift Tensors (parts per million) for Semiquinone Complexes[a]

structure	Δg_{iso}	Δg_x	Δg_y	Δg_z
$BQ^{-\bullet}$, opt.	3010	6048	3001	−21
$BQ^{-\bullet}$−indole, opt., T-stacked[b]	3250	6498	3213	40
$BQ^{-\bullet}$−indole, X-ray[c]	3022	5963	3074	28
$BQ^{-\bullet}$−$(H_2O)_2$, opt., T-stacked[b]	3219	6215	3364	78
$DQ^{-\bullet}$, opt.	2721	5202	2976	−14
$DQ^{-\bullet}$−indole, opt., T-stacked[b]	2954	5644	3171	47
$DQ^{-\bullet}$−indole, X-ray[c]	2672	5026	2953	36
$DMNQ^{-\bullet}$, opt.	2486	4666	2790	1
$DMNQ^{-\bullet}$−indole, opt., T-stacked[b]	2673	4975	2986	58
$DMNQ^{-\bullet}$−indole, X-ray[c]	2490	4609	2822	39
$DMNQ^{-\bullet}$−nmf, X-ray[c]	2355	4341	2722	2
$DMNQ^{-\bullet}$−indole−nmf, X-ray[c]	2316	4227[d]	2707[d]	14[d]

[a] UDFT/BP86 results. nmf is *N*-methylformamide (taken as a model for a protein backbone N−H function). Slightly different values compared to those from ref *8* for the isolated semiquinones result from the different structures (MP2-optimized vs DFT-optimized). [b] Fully optimized, perpendicular complexes (T-stacked hydrogen bonding). [c] Intermolecular distances and relative orientations have been taken from the (π-stacked) X-ray structure of PS-I (*10*), but fragment structures were MP2-optimized. [d] For an N−H···O distance of 1.854 Å. Calculations with a more realistic, optimized N−H···O hydrogen bond distance of 1.724 Å give the following values: $\Delta g_x = 4194$ ppm, $\Delta g_y = 2687$ ppm, and $\Delta g_z = -3$ ppm.

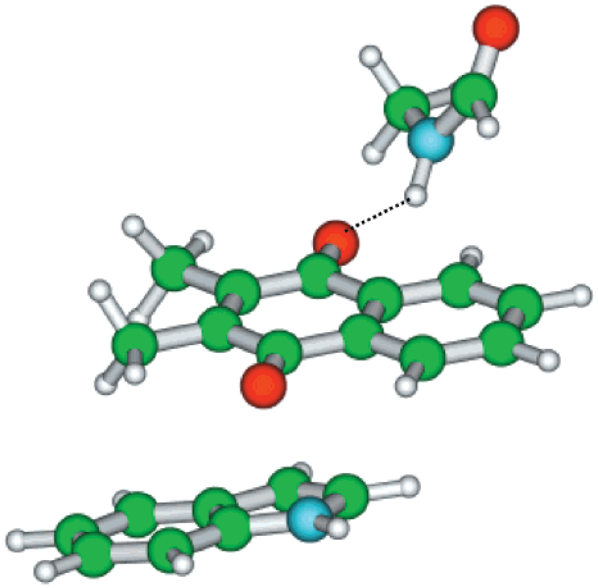

FIGURE 3: Structure employed for the $DMNQ^{-\bullet}$−indole−nmf model complex. The intermolecular orientation and position were taken from the recent X-ray analysis of PS-I (*10*), but MP2-optimized parameters were used for the fragments. $DMNQ^{-\bullet}$ replaces $Q_K^{-\bullet}$, indole Trp A677, and nmf Leu A722.

2) (further interactions are expected to favor the semiquinone state even more; see below). Attempts to carry out constrained optimizations on the $BQ^{-\bullet}$−indole complex, with the non-hydrogen atoms of the indole being forced to stay parallel to the semiquinone plane, led to arrangements with the pyrrole ring shifted away from the semiquinone, and with the indole N−H bond bent down to form an incipient hydrogen bond to one of the semiquinone oxygen atoms (structure not shown). This provides a further indication that semiquinones strongly prefer to avoid a parallel π-stacked arrangement with an indole, and that T-stacked hydrogen bonding to the π-system of semiquinones is a much more favorable interaction.

Table 3 compares the **g**-shift tensors calculated for the isolated semiquinones and for their complexes with indole in various structural arrangements. In the parallel π-stacked orientation observed in the X-ray structure analysis (*10*), the presence of an indole actually *decreases* Δg_x slightly. The Δg_y component is either increased or decreased by a relatively small amount. Thus, $\pi-\pi$ interactions influence the **g**-tensors of semiquinones only little, and they certainly cannot account for the large Δg_x and Δg_y components of $DQ^{-\bullet}$ or $NQ^{-\bullet}$ in PS-I (Table 1), or even for the relatively large Δg_x in native PS-I. Table 3 shows furthermore that the hydrogen bond to a leucine (Leu) residue in PS-I [modeled by a complex of $DMNQ^{-\bullet}$ with *N*-methylformamide (nmf) at the position of Leu A722 in the X-ray structure of PS-I[2] (*10*)] causes a significant reduction in Δg_x and a smaller reduction in Δg_y, as found previously for related hydrogen-bonded complexes (*8*). Our most realistic model for $Q_K^{-\bullet}$ in the A_1 binding site is provided by the $DMNQ^{-\bullet}$−indole−nmf complex (Table 3; cf. Figure 3). After scaling Δg_x by 0.92 to account for the systematic DFT errors (*8*), the computed **g**-tensor for this model is in excellent agreement with the experimental data (*6*, *7*) for $Q_K^{-\bullet}$ in PS-I (Table 1). This suggests that the position of the semiquinone in this case is very similar to that of the neutral quinone in the X-ray structure, consistent with the conclusions from several EPR studies (*4*, *6*, *7*, *13*, *26*, *27*). An optimization of the $DMNQ^{-\bullet}$−nmf interaction provides a lower, more realistic (*8*) N−H···O hydrogen bond length of 1.724 Å. However, the calculated **g**-tensor data for this structure are almost identical to those obtained for the experimental intermolecular distances (Table 3).

While $\pi-\pi$ interactions with an indole obviously have a quite small effect on the **g**-tensors of the semiquinones, the fully optimized, T-stacked $Q^{-\bullet}$−indole complexes (cf. Figure 2) exhibit an increase in Δg_x and Δg_y of ~6−8% ppm compared to those of the free radical anions (Table 3). This is not enough to explain fully the very large Δg_x and Δg_y components for $DQ^{-\bullet}$ or $NQ^{-\bullet}$ in PS-I (Table 1) (*3*, *4*). However, it shows that perpendicular H-bonds to the π-system of semiquinones increase both Δg_x and Δg_y significantly, in striking contrast to hydrogen bonding to the carbonyl oxygen atoms. We believe that the very large enhancement of Δg_x and Δg_y measured for the reconstituted systems reflects one or two further H-bonds to the π-system (see below). For example, Table 3 shows the **g**-shift tensor for a complex with two water molecules T-stacked to $BQ^{-\bullet}$ from opposite sides. Again, the T-stacked hydrogen bonds lead to a significant enhancement of both Δg_x and Δg_y. We have probed the dependence of the **g**-shifts on structure in detail for $BQ^{-\bullet}$−H_2O models (data not shown) and find the largest effects on both Δg_x and Δg_y when several hydrogen bonds are positioned above the central part of the semiquinone ring. Most importantly, T-stacked hydrogen bonds appear to be essential to enhancing Δg_y. No obvious alternative explanation is foreseeable for the large Δg_y values of the above preparations with $DQ^{-\bullet}$ or $NQ^{-\bullet}$ in the A_1 site, unless unrealistically large interactions with charged amino acid residues are invoked.

These results indicate the following. While quinones prefer a parallel, π-stacked interaction with Trp residues, their semiquinone radical anions preferentially interact in an N−H···π bonded, T-stacked arrangement. In the case of

quinones with extended side chains such as Q_K, the A_1 quinone binding site apparently does not allow the reorientation upon reduction that would be required for optimum stabilization of the semiquinone. Therefore, the Trp−$Q_K^{-\bullet}$ interaction is less favorable than the Trp−Q_K interaction. This corresponds to a modest lowering of the redox potential in the A_1 site. From our computed binding energies in Table 2, we conservatively estimate the change to be between 50 and 150 mV (cf. the discussion above).

The redox potential of Q_K in PS-I is ca. −750 to −810 mV (*1*, *2*), versus ca. −150 to ca. −250 mV for phylloquinone in protic solvents (*28*). Obviously, the Trp−Q_K interactions cannot be solely responsible for these differences. Compared to the binding sites of type II reaction centers or to a protic solution, the sparse hydrogen bonding to just one Leu residue is expected to provide another lowering of the redox potential. DFT calculations have suggested (*29*) that one strong hydrogen bond to a carbonyl oxygen atom accounts for an increase in $Q/Q^{-\bullet}$ reduction potentials of at least ∼250 mV. Considering an average number of possibly three hydrogen bonds in protic solution compared to one strong hydrogen bond in PS-I, and taking into account that the average number of hydrogen bonds in solution is probably larger for the semiquinone than for the quinone (*30*), we expect a lowering of the $Q_K/Q_K^{-\bullet}$ redox potential in PS-I of possibly up to ∼500 mV [note that redox potentials of some closely related quinones in the aprotic DMF solvent are ca. −460 to ca. −480 mV (*31*)]. Augmented by a ca. 50−150 mV decrease in the redox potential due to Trp−Q_K π-stacking interactions, these differences in hydrogen bonding easily account for the very low redox potential in the A_1 site. Due to the very small difference between the $Q_K/Q_K^{-\bullet}$ redox potential and that of the next acceptor (*1*, *2*), the iron−sulfur cluster F_x, the modest extra energy contributions from the Trp−Q_K interaction may, however, be essential in enabling forward electron transfer beyond Q_K. Note that π-stacking with a Trp residue is also observed for the quinone Q_A in bacterial reaction centers (*32*). However, in this case, the π-stacking appears to be weaker, and reorientation of semiquinones is unlikely, because of strong hydrogen bonding to the semiquinone oxygen atoms.

In contrast to Q_K, a smaller quinone without an extended side chain apparently is able, upon reduction to the semiquinone, to adjust its position within the (reconstituted and thus modified[3]) A_1 binding site to enhance the interaction energy of the radical anion in a T-stacked hydrogen bonding arrangement. Inspection of the recently reported high-resolution crystal structure of PS-I (*10*) allows us to estimate what type of reorientation is most likely. To enable a T-stacked $Q^{-\bullet}$−Trp A697[2] arrangement, the N−H···O hydrogen bond from Trp to nearby Ser A692[2] has to be broken (cf. Figure 4). This could easily be replaced by an N−H···OH hydrogen bond from Gly A693[2] to Ser A692[2]. More likely, however, the semiquinone will insert between residues A697, A692, and A693, thus accepting up to three T-stacked H-bonds into its π-system. These would be (i) the N−H···π bond from Trp A697, (ii) the O−H···π bond from Ser A692, and (iii) the N−H···π bond from the backbone N−H of Gly A693. This requires a <90° reorientation of the semiquinone compared to its original position, as well as relatively minor adjustments of the relevant amino acid residues (Figure 4). Due to the negative charge of the semiquinone, multiple T-stacking interactions are expected to overcompensate for the rearrangement of some other hydrogen bonds, including that from Leu A722[2] to a carbonyl oxygen atom of the semiquinone. For example, in our calculations of the $BQ^{-\bullet}$−indole−nmf model complex, the T-stacked H-bond donated by nmf accounts for an energy gain of ∼42 kJ/mol (CP-corrected MP2 data), which together with the T-stacked hydrogen bond from indole leads to a remarkable overall stabilization by ∼94 kJ/mol. This type of highly favorable reorientation appears to be the most likely "least-motion" scenario for $NQ^{-\bullet}$ or $DQ^{-\bullet}$ within the reconstituted A_1 site (see above). The present data cannot exclude alternative models, e.g., arrangements involving water molecules [cf. the large Δg_x and Δg_y for the $BQ^{-\bullet}$−$(H_2O)_2$ model in Table 1], or other H-bond donors. In any case, the measured and computed **g**-tensors provide strong support for T-stacking in the reconstituted systems. A referee has suggested that, if a T-stacked arrangement occurred in the reconstituted preparations, it might already have been identified by a very large hyperfine coupling constant. This is not the case. For the T-stacked $DMNQ^{-\bullet}$−indole complex, our calculations of the **A**-tensor at the B3LYP/EPR-II density functional level give the following values: $A_{11} = -3.87$ MHz, $A_{22} = 1.33$ MHz, and $A_{33} = 1.83$ MHz. This is an unremarkable hyperfine tensor and probably could not be resolved in the EPR studies (*3*, *4*). Similarly, our calculated nitrogen hyperfine and nuclear quadrupole coupling tensors for the indole nitrogen atom (data not shown) do not suggest characteristic differences between the π- and T-stacked arrangement. The **g**-tensors appear to be the most sensitive probe of the different interaction modes. Further studies of hyperfine, nuclear quadrupole, and **g**-tensors are currently underway in our laboratory.

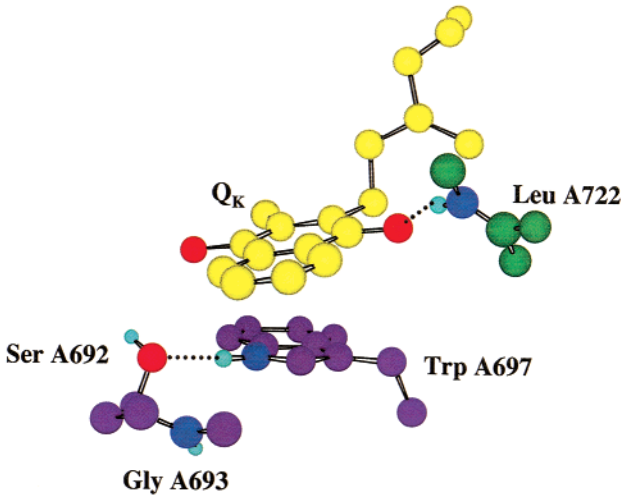

FIGURE 4: Display of the local protein environment of Q_K in the A_1 site of PS-I (A branch) (*10*). The carbon atoms have been color-coded for the quinone (yellow), Leu A722 (green), and those residues most likely involved in T-stacked interactions to semiquinones without an extended side chain (magenta). The side chain of the quinone has been truncated, and only those hydrogen atoms involved in hydrogen bonding are shown.

[3] The extraction and reconstitution studies employed methanol/hexane mixtures for extraction of phylloquinone. Modifications of the A_1 site by this procedure cannot be excluded. Somewhat different results appear to arise from extractions with ether solvents (*11*).

There are several further experimental observations that may be rationalized by the proposed model. (i) In the PS-I reaction centers reconstituted with DQ or NQ, the quinone still acts as an electron acceptor toward P700*, but the forward electron transfer to F_x is blocked. This holds also for other quinones without an extended side chain (*33*) and is consistent with an increased redox potential, due to the reorientation and T-stacking of the semiquinone. Consequently, in biochemical studies, these reconstituted reaction centers are not capable of $NADP^+$ photoreduction (*34*). (ii) EPR measurements for PS-I complexes of *menA* and *menB* interruption mutants of *Synechocystis* PCC 6803 indicate the recruitment of a plastoquinone-9 (PQ-9) into the A_1 site, instead of the missing Q_K. The data show that the orientation of $PQ\text{-}9^{-\bullet}$ in either the photoaccumulated or charge-separated radical state is identical to that of $Q_K^{-\bullet}$ in native PS-I. The **g**-tensor (*35*) does not reveal any sign of T-stacked interactions with the nearby Trp residue (no large Δg_y values). It appears that PQ-9, which bears an extended side chain, does not reorient upon reduction. Notably, in these preparations, forward electron transfer to F_x functions. After submission of the initial version of this work, a study of *menG* mutants has been reported (*36*). Here 2-phytyl-1,4-naphthoquinone replaces Q_K. Despite the lack of the 3-methyl group, the orientation of the semiquinone in the binding site appears to be unaltered. The redox potential and electron transfer characteristics are slightly modified compared to those of the wild-type protein, but the overall function is not affected dramatically. (iii) Site-directed mutagenesis of Trp residues PsaA W693 and PsaB W673 in *Chlamydomonas reinhardtii* (which correspond to Trp A697 and B677, respectively, in *S. elongatus*) slows individually the two phases of forward electron transfer (*14*).

The results presented here are relevant beyond the specific case of photosystem I. They highlight for the first time the possible importance of T-stacked hydrogen bonding interactions to semiquinones, compared to a preference for π-stacking of neutral quinones with aromatic amino acid residues. It appears likely that nature can choose between these different intermolecular interactions to appropriately adjust redox potentials in electron transfer processes involving quinones. These processes are ubiquitous in living organisms.

ACKNOWLEDGMENT

Helpful discussions with Drs. R. Bittl (Berlin, Germany), I. Ciofini (Würzburg, Germany), V. G. Malkin, O. L. Malkina (Bratislava, Slovak Republic), J. Vaara (Helsinki, Finland), F. MacMillan (Frankfurt, Germany), and D. Stehlik (Berlin, Germany) are gratefully acknowledged. T. Gress is thanked for carrying out some of the calculations.

REFERENCES

1. Brettel, K. (1997) *Biochim. Biophys. Acta 1318*, 322−373.
2. Brettel, K., and Leibl, W. (2001) *Biochim. Biophys. Acta 1507*, 100−114.
3. Sieckmann, I., van der Est, A., Bottin, H., Sétif, P., and Stehlik, D. (1991) *FEBS Lett. 284*, 98−102.
4. van der Est, A., Sieckmann, I., Lubitz, W., and Stehlik, D. (1995) *Chem. Phys. 194*, 349−359.
5. Burghaus, O., Plato, M., Rohrer, M., Möbius, K., MacMillan, F., and Lubitz, W. (1993) *J. Phys. Chem. 97*, 7639−7646.
6. MacMillan, F., Hanley, J., van der Weerd, L., Knüpling, M., Un, S., and Rutherford, A. W. (1997) *Biochemistry 36*, 9297−9303.
7. Zech, S. G., Hofbauer, W., Kamlowski, A., Fromme, P., Stehlik, D., Lubitz, W., and Bittl, R. (2000) *J. Phys. Chem. B 104*, 9728−9739.
8. Kaupp, M., Remenyi, C., Vaara, J., Malkina, O. L., and Malkin, V. G. *J. Am. Chem. Soc.* (in press).
9. Malkina, O. L., Vaara, J., Schimmelpfennig, B., Munzarová, M., Malkin, V. G., and Kaupp, M. (2000) *J. Am. Chem. Soc. 122*, 9206−9218.
10. Jordan, P., Fromme, P., Witt, H. T., Klukas, O., Saenger, W., and Krauss, N. (2001) *Nature 411*, 909−917.
11. Iwaki, M., and Itoh, S. (1991) *Biochemistry 30*, 5347−5352.
12. Hanley, J., Deligiannakis, Y., MacMillan, F., Bottin, H., and Rutherford, A. W. (1997) *Biochemistry 36*, 11543−11549.
13. Kamlowski, A., Altenberg-Greulich, B., van der Est, A., Zech, S. G., Bittl, R., Fromme, P., Lubitz, W., and Stehlik, D. (1998) *J. Phys. Chem. B 102*, 8278−8287.
14. Guergova-Kuras, M., Boudreaux, B., Joliot, A., Joliot, P., and Redding, K. (2001) *Proc. Natl. Acad. Sci. U.S.A. 98*, 4437−4442.
15. Purton, S., Stevens, D. R., Muhiuddin, I. P., Evans, M. C. W., Carter, S., Rigby, S. E. J., and Heathcote, P. (2001) *Biochemistry 40*, 2167−2175.
16. Frisch, M. J., et al. (1998) *Gaussian 98*, revisions A.7 and A.9, Gaussian, Inc., Pittsburgh, PA.
17. Bergner, A., Dolg, M., Küchle, W., Stoll, H., and Preuss, H. (1993) *Mol. Phys. 80*, 1431.
18. Godbout, N., Salahub, D. R., Andzelm, J., and Wimmer, E. (1992) *Can. J. Chem. 70*, 560−571.
19. Boys, S. F., and Bernardi, F. (1970) *Mol. Phys. 19*, 553−566.
20. Becke, A. D. (1988) *Phys. Rev. A 38*, 3098−3100.
21. Perdew, J. P. (1986) *Phys. Rev. B 33*, 8822−8824.
22. Salahub, D. R., Fournier, R., Mlynarski, P., Papai, I., St-Amant, A., and Ushio, J. (1991) in *Density Functional Methods in Chemistry* (Labanowski, J., and Andzelm, J., Eds.) Springer, New York.
23. Hess, B. A., Marian, C. M., Wahlgren, U., and Gropen, O. (1996) *Chem. Phys. Lett. 251*, 365−371.
24. Schimmelpfennig, B. (1996) *Atomic Spin−Orbit Mean-Field Integral Program*, Stockholms Universitet, Stockholm, Sweden.
25. Bühl, M., Kaupp, M., Malkin, V. G., and Malkina, O. L. (1999) *J. Comput. Chem. 20*, 91−105.
26. van der Est, A., Prisner, T. F., Bittl, R., Fromme, P., Lubitz, W., Möbius, K., and Stehlik, D. (1997) *J. Phys. Chem. B 101*, 1437−1443.
27. Bittl, R., Zech, S. G., Fromme, P., Witt, H. T., and Lubitz, W. (1997) *Biochemistry 36*, 12001−12004.
28. Swallow, A. J. (1982) in *Function of Quinones in Energy Conserving Systems* (Trumpower, B. L., Ed.) pp 59−72, Academic Press, New York.
29. O'Malley, P. J. (1999) *Biochim. Biophys. Acta 1411*, 101−113.
30. Nilsson, J. A., Lyubartsev, A., Eriksson, L. A., and Laaksonen, A. (2001) *Mol. Phys. 99*, 1795−1804.
31. Prince, R. C., Dutton, P. L., and Bruce, J. M. (1983) *FEBS Lett. 160*, 273−276.
32. Stowell, M. H. B., McPhillips, T. M., Rees, D. C., Soltis, S. M., Abresch, E., and Feher, G. (1997) *Science 276*, 812−816.
33. Rustandi, R. R., Snyder, S. W., Biggins, J., Norris, J. R., and Thurnauer, M. C. (1992) *Biochim. Biophys. Acta 1101*, 311−320.
34. Biggins, J., and Mathis, P. (1988) *Biochemistry 27*, 1494−1500.
35. Zybailov, B., van der Est, A., Zech, S. G., Teutloff, C., Johnson, T. W., Shen, G., Bittl, R., Stehlik, D., Chitnis, P. R., and Golbeck, J. H. (2000) *J. Biol. Chem. 275*, 8531−8539.
36. Sakuragi, Y., Zybailov, B., Shen, G., Jones, A. D., Chitnis, P. R., van der Est, A., Bittl, R., Zech, S., Stehlik, D., Golbeck, J. H., and Bryant, D. A. (2002) *Biochemistry 41*, 394−405.

BI0159783